Chemosphere 304 (2022) 135311

Contents lists available at ScienceDirect

Chemosphere

journal homepage: www.elsevier.com/locate/chemosphere

Adsorption of recalcitrant phosphorus compounds using the phosphate-selective binding-protein PstS

Synthia P. Mallick [a], Faten B. Hussein [a], Shayla Husted [b], Brooke K. Mayer [a,*]

[a] Department of Civil, Construction and Environmental Engineering, Marquette University, 1637 West Wisconsin Avenue, Milwaukee, WI, 53233, USA
[b] Department of Biological Sciences, Marquette University, 1428 W. Clybourn St., Milwaukee, WI, 53233, USA

HIGHLIGHTS

- PBP effectively adsorbed [in]organic soluble non-reactive phosphorus (sNRP).
- Adsorption of sNRP compounds on PBP was thermodynamically favorable.
- The immobilized PBP rapidly adsorbed sNRP.
- Greater P removal was observed for compounds with higher P content.
- Adsorption followed a Langmuir isotherm and desorption was high at pH 12.

GRAPHICAL ABSTRACT

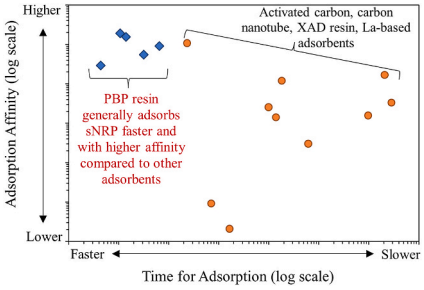

ARTICLE INFO

Handling Editor: Y Yeomin Yoon

Keywords:
Phosphate-binding protein (PBP)
Soluble non-reactive phosphorus (sNRP)
Resource recovery
Organic
Pseudo-second order (PSO) kinetics
Affinity

ABSTRACT

Currently available wastewater phosphorus (P) treatment technologies target removal of reactive forms of P. Selective adsorption of more recalcitrant soluble non-reactive phosphorus (sNRP) can improve P removal and recovery. A phosphate-selective phosphate-binding protein (PBP), PstS, was immobilized onto NHS-activated beads to assess the ability of this novel bioadsorbent to remove (adsorb) and subsequently recover (desorb) a range of sNRP compounds. Four sNRP compounds representative of wastewater sNRP were selected for use in this study: phytic acid (PA), sodium triphosphate (TrP), beta-glycerol phosphate (BGP), and sodium hexametaphosphate (HMP). Using PBP, adsorption of all sNRP compounds was thermodynamically favorable. The PBP had nearly equivalent binding affinity for PA compared to PBP's typical target, orthophosphate, although it had less affinity for the other sNRP compounds. Adsorption followed pseudo-second order reaction kinetics, with 95% of maximum adsorption occurring within 4 min. This was substantially faster sNRP adsorption compared to other adsorbents in the literature. Adsorption was modeled using the Langmuir isotherm, reflecting that one phosphate molecule attached to one PBP binding site. Notably, this selective 1:1 attachment resulted in higher total P removal for sNRP molecules with high P content. The binding site lost activity with increasing pH, and as such, highest desorption was achieved at pH 12, making the system amenable to sNRP removal as well as controlled recovery.

* Corresponding author.
E-mail addresses: Synthiaparveen.Mallick@Marquette.edu (S.P. Mallick), Faten.Hussein@Marquette.edu (F.B. Hussein), Shayla.Husted@Marquette.edu (S. Husted), Brooke.Mayer@Marquette.edu (B.K. Mayer).

https://doi.org/10.1016/j.chemosphere.2022.135311
Received 18 April 2022; Received in revised form 8 June 2022; Accepted 9 June 2022
Available online 13 June 2022
0045-6535/© 2022 Elsevier Ltd. All rights reserved.

Abbreviations

BGP	Beta-glycerol phosphate
HMP	Sodium hexa-metaphosphate
IPTG	Isopropyl ß-D-1-thiogalactopyranoside
ITC	Isothermal titration calorimetry
K_B	Ligand-protein binding constant
K_D	Ligand-protein dissociation constant
K_F	Freundlich isotherm constant
K_L	Langmuir isotherm constant
K_{PFO}	Reaction constant for pseudo-first order reaction
K_{PSO}	Reaction constant for pseudo-second order reaction
LB	Luria broth
MDL	Minimum detection limit
MWCO	Molecular weight cutoff
NHS	N-hydroxy-succinimide
PA	Phytic acid
PFO	Pseudo-first order
P	Phosphorus
P_i	Reactive phosphorus, or orthophosphate
PSO	Pseudo-second order
q_e	Adsorption capacity at equilibrium
q_{max}	Maximum adsorption capacity
SDS-PAGE	Sodium dodecyl sulfate–polyacrylamide gel electrophoresis
SEC	Size exclusion chromatography
sNRP	Soluble non-reactive phosphorus
sRP	Soluble reactive phosphorus
TEP	Triethyl phosphate
TP	Total phosphorus

1. Introduction

Phosphorus (P) is the limiting nutrient in most freshwater ecosystems, such that excess P in surface waters can cause harmful algal blooms or eutrophication (Carpenter, 2008). Major sources of P release into surface waterbodies can include stormwater run-off of agricultural P products or wastewater-derived P discharge (Drolc and Zagorc Koncan, 2002). Reducing P discharges into surface waterbodies is therefore critical. Water resource reclamation facilities (WRRFs) may need to consider advanced treatment to reduce P discharge as much as possible (Mayer et al., 2016). Beyond P removal, recovery of wastewater-derived P can enhance P sustainability as non-renewable mineral P resources are depleted to meet increasing fertilizer demands (Reijnders, 2014). A circular P economy recovering waste P for reuse as fertilizer is therefore important to meet both environmental protection goals and sustain high levels of global food production.

Conventional biological and physical-chemical wastewater treatment processes used for P treatment include enhanced biological P removal, adsorption, ion exchange, chemical precipitation, micro- or ultra-filtration, and coagulation/flocculation/sedimentation (Morse et al., 1998). However, only particulate P and the reactive form of P (primarily consisting of orthophosphate) are generally removed using these conventional treatment processes (Venkiteshwaran et al., 2018a). Reactive P is defined as being detectable in a colorimetric test, whereas the remaining P, classified as non-reactive P, must undergo hydrolysis or oxidation to make it detectable (APHA, 2012). Gu et al. (2011) showed that conventional P treatment typically removes less than 40% of soluble non-reactive P (sNRP). Consequently, approximately 26–81% of wastewater effluent P can be in the more recalcitrant sNRP form (Qin et al., 2015). Following effluent discharge to environmental waters, sNRP can be transformed through enzymatic processes or photolysis, or directly utilized by microbes in a reactive-P-limited aquatic environment (Qin et al., 2015; Venkiteshwaran et al., 2018a). For example, Qin et al. (2015) demonstrated approximately 75% utilization of effluent sNRP for algal biomass growth. Therefore, developing technologies to effectively remove sNRP from wastewater is critical to reduce P discharge and the associated negative effects.

Currently, sNRP removal studies are limited, and focus primarily on advanced oxidation processes (AOPs). Removal, detoxification, or transformation of sNRP compounds using AOPs such as UV/H_2O_2, UV/TiO_2, Fenton, photo-Fenton, and electrooxidation has been reported (Badawy et al., 2006; Daneshvar et al., 2004; Gray et al., 2020; Mallick et al., 2021; Sindelar et al., 2016; Venkiteshwaran et al., 2021a).

Adsorption offers another route to achieve effective sNRP removal without direct energy inputs, but there are currently limited reports of sNRP adsorption/desorption efficiency. Long contact times were needed to remove sNRP using hierarchical porous magnesium oxide (Hr-MgO), granular activated carbon (GAC), powdered activated carbon (PAC), carbon nanotubes, XAD resin, and lanthanum (La)-based adsorbents (Campos do Lago et al., 2020; Xu et al., 2020; Sharma and Kakkar, 2017; Wang et al., 2018b, 2018a). Most of these studies reported that the time to reach adsorption equilibrium ranged from hours to longer than a day (although adsorption of triphenyl phosphate on PAC was faster, at approximately 15 min). An additional consideration is that these materials are non-selective for sNRP or other P species. This may negatively impact adsorption efficiency and limits the potential to recover pure P products.

Resins with selectivity for orthophosphate, or reactive phosphorus (P_i), (e.g., LayneRT or phosphate-binding protein resin) may offer a means to adsorb sNRP compounds, particularly those compounds with phosphate functional groups, while minimizing non-target adsorption. However, evaluations of the adsorption potential of sNRP compounds on P-selective materials is lacking. In this study, we assessed the adsorption/desorption potential of sNRP using a promising protein-based phosphate-selective adsorbent featuring immobilized PstS phosphate-binding proteins (PBP).

The P-selective PBP PstS is an integral part of the high-affinity phosphate-specific transporter system expressed naturally by many microorganisms when P_i concentrations are low. The protein's ability to adsorb monobasic ($H_2PO_4^-$) and dibasic (HPO_4^{2-}) P_i (Wang et al., 1994) even at low levels makes it attractive for use in systems targeting ultra-low effluent P concentrations. The PBP sequesters P_i in a deep cleft using 12 strong hydrogen bonds formed between the phosphate molecule's 4 oxygen atoms and the protein's amino acid residues (Luecke and Quiocho, 1990). These interactions yield PBP's exquisite P_i-specificity (Luecke and Quiocho, 1990), which has been harnessed to remove and recover P_i using both proteins in microbial cells and extracted proteins immobilized on resins suitable for flow-through filter operation (Hussein and Mayer, 2022; Venkiteshwaran et al., 2018b, 2021b; Yang et al., 2016; Choi et al., 2013; Li et al., 2009; Kuroda et al., 2000). Notably, immobilized PBP adsorbents offer faster adsorption and greater P_i selectivity compared to metal-oxide P_i-selective materials, including LayneRT P_i-selective ion exchange material (Hussein and Mayer, 2022; Venkiteshwaran et al., 2020), but have yet to be tested for sNRP removal/recovery. Recalcitrant sNRP compounds with accessible phosphate functional groups may be able to bind to PBP's active site, facilitating removal, followed by pH adjustment to stimulate sNRP release, facilitating recovery (Venkiteshwaran et al., 2020). Therefore, the objectives of this study were to: (1) assess sNRP adsorption efficiency using immobilized PBP, including testing sNRP binding affinity, kinetics, adsorption isotherms, thermodynamics, and competition between P_i and sNRP; and (2) evaluate the recoverability of adsorbed sNRP compounds through desorption experiments.

2. Materials and methods

2.1. sNRP compounds

Four sNRP compounds were selected to represent different types of wastewater sNRP (e.g., organic and inorganic compounds with cyclic or simple structure): beta-glycerol phosphate (BGP), phytic acid (PA), sodium triphosphate (TrP), and sodium hexametaphosphate (HMP) (Fig. 1). BGP is a simple organic compound whereas PA is a cyclic organic compound. Among the inorganic sNRP compounds tested, TrP has a simple structure while HMP has a complex cyclic structure. All compounds were 99% pure, and purchased from Sigma Aldrich (St. Louis, MO). All sNRP solutions were made by spiking Tris buffer (10 mM Tris-HCl, 1 mM $MgCl_2$, pH 7) with sNRP at an initial concentration of 0.36 ± 0.02 mg P/L. During the adsorption isotherm experiments, a range of sNRP concentrations were tested: 0.075, 0.1, 0.2, 0.25, 0.3, and 0.35 mg P/L. Low concentrations were used to assess the adsorption capacity of PBP resin targeting removal of total phosphorus (TP) from initially low levels to ultra-low levels (i.e., tertiary treatment to satisfy ultra-low discharge regulations).

2.2. PBP resin preparation

The adsorption and desorption experiments were conducted using immobilized PBP (PBP resin) as immobilized PBP is better suited for wastewater treatment applications. The PBP resin was prepared by expressing, purifying, and immobilizing PBP on NHS-activated Sepharose beads, in accordance with protocols described by Venkiteshwaran et al. (2018b). Briefly, His-tagged PBP was over-expressed into *E. coli* BL21 (DE3) cells (Thermo Fisher Scientific, Waltham, MA) grown in Luria broth (LB) using isopropyl β-D-1-thiogalactopyranoside (IPTG). After 4-h at 35 °C, cells were centrifuged and the cell pellets were collected and stored at 4 °C. Over-expression of PBP was confirmed using SDS-PAGE. Cell pellets were resuspended in a binding buffer (50 mM NaH_2PO_4, 500 mM NaCl, 10 mM imidazole, pH 6) and lysed via sonication at 45% amplitude and a pulse rate of 15 s on and 45 s off (Q500 sonicator, QSonica, Newtown, CT). The solution was then centrifuged (1000 rpm, 6700×*g*) to remove cellular debris. The supernatant containing PBP was added to a Ni^{2+} column (Ni Sepharose™ 6 Fast Flow, Cytiva, Marlborough, MA) containing the binding buffer and gently mixed for 1 h. The Ni^{2+} column was then rinsed 5 times using an elution buffer at pH 8. The elution buffer consisted of 137.5 mL of purification buffer (50 mM NaH_2PO_4, 500 mM NaCl) and 12.5 mL of 3 M imidazole. An SDS-PAGE gel was used to confirm the presence of purified PBP. Purified PBP was then dialyzed in a dialysis buffer (0.2 M $NaHCO_3$, 0.5 M NaCl, pH 8) for 4.5 h and stored in 70% glycerol at −80 °C (volumetric ratio of PBP to glycerol was 4 to 1). The purified PBP concentration was 9.4 ± 0.3 mg/mL, as measured using a Pierce™ BCA Protein Assay Kit (Thermo Fisher Scientific, Waltham, MA).

To immobilize PBP on the NHS-activated Sepharose 4 Fast Flow beads (Cytiva, Marlborough, MA), purified PBP was first dialyzed for 4.5 h in the dialysis buffer using a Spectra/Por 2 dialysis membrane (MWCO 12–14 kDa, Spectrum Laboratories Inc., Rancho Dominguez, CA) to remove the glycerol storage solution. The NHS beads were prepared following the manufacturer's protocol (71-5000-14AAD, Cytiva, Marlborough, MA). Dialyzed PBP was added to the NHS beads and gently mixed for 4 h. After 4 h, the solution was drained and the PBP resin was washed 3 times using acid (0.1 M Na-acetate, 0.5 M NaCl, pH 4.5) and base (0.1 M Tris-HCl, pH 8) solutions. The PBP resin was stored in storage buffer (10 mM Tris-HCl, 1 mM $MgCl_2$, pH 7) at 4 °C for up to 48 h prior to experimentation. Before experiments, PBP resin was washed in storage buffer at pH 7 and pH 12. The alkaline buffer solution removed residual P from the PBP resin. The PBP resin was then resuspended in an equal bed volume of storage buffer at pH 7. The concentration of PBP was measured using a Pierce™ BCA Protein Assay Kit before and after attachment to determine attachment efficiency on the NHS beads. The PBP concentration on the NHS beads ranged from 15.6 to 16.5 nmol/mL. Ultrapure water (resistivity of 18.2 MΩ*cm at 25 ± 1 °C, Elga, High Wycombe, UK) was used to prepare all solutions and buffers.

2.3. PBP binding affinity for sNRP compared to P_i

The PBP's affinity for different sNRP compounds was evaluated using isothermal titration calorimetry (ITC) (performed by Charles River Laboratories, Essex, UK). Briefly, refolded PBP was dialyzed in size exclusion chromatography (SEC) buffer (20 mM Na-HEPES, 150 mM NaCl, pH 7.4). In individual experiments, 0.5–5 mM of each P compound (PA, BGP, HMP, TrP, or P_i) was titrated with 50 μM PBP in SEC buffer at 25 °C. Changes in heat, or enthalpy (ΔH, kJ/mol), were measured using a VP-ITC MicroCalorimeter (MicroCal Incorporated, Commerce, CA). A plot of ΔH versus molar ratio was used to calculate the dissociation

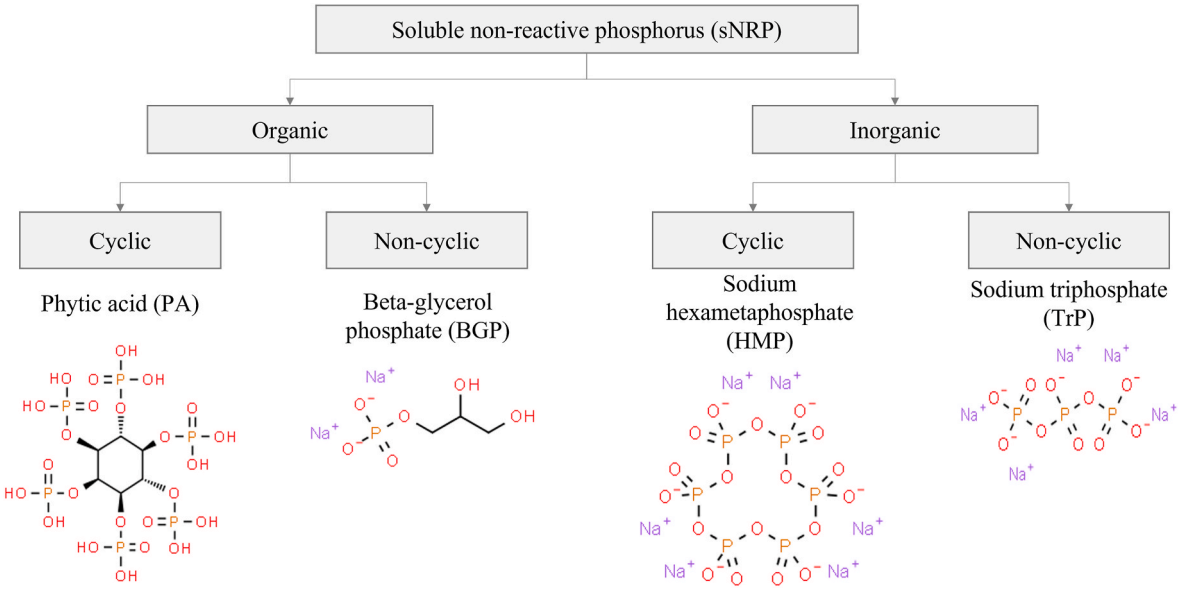

Fig. 1. Selected soluble non-reactive phosphorus (sNRP) compounds tested in this study. Different types of compounds (organic, inorganic, cyclic, non-cyclic) were tested to represent a range of wastewater sNRP compounds. All chemical structure images were taken from Chemspider.

constant, K_D, and change in entropy (ΔS, kJ/mol-K). For protein-ligand binding, the lower the K_D value, the higher the protein's affinity to bind with the ligand. The thermodynamic feasibility of binding (change in Gibb's free energy, $\Delta G = \Delta H - T\Delta S$, where T = temperature in K and ΔG is quantified in kJ/mol) was calculated using the ΔH and ΔS values to provide an indicator of thermodynamic feasibility of the binding reaction (signified by negative ΔG).

2.4. Adsorption (kinetics, isotherms, competition) and desorption experiments

Kinetic experiments were conducted using 15.6–17.3 nmol PBP (1.3 mL of PBP resin suspension) together with 10.5 mL of sNRP solution (pH 7) containing 0.36 ± 0.02 mg P/L mixed on a Multi-Purpose Tube Rotator at 20 rpm (Thermo Fisher Scientific, Waltham, MA). To determine how quickly sNRP compounds adsorbed, independent batch experiments were run for 0.5, 1, 2, 5, 10, and 20 min.

Isotherm experiments were conducted using 16.6 nmol PBP (1.3 mL PBP resin suspension) together with 10.5 mL of sNRP solution (pH 7) containing different P concentrations: 0.071, 0.106, 0.204, 0.242, 0.301, and 0.363 mg P/L. These experiments were conducted for 10 min (sufficient to achieve equilibrium, as indicated by the kinetic experiments).

To assess for competition between P_i and the sNRP compounds, a pH 7 buffer containing varying ratios of sNRP to P_i (20%, 60%, 70%, or 100% TP as sNRP) was exposed to 21 nmol PBP for 10 min.

Phosphorus desorption experiments were conducted by first adsorbing sNRP onto 21 nmol PBP resin for 10 min at pH 7. After 10 min, the solution was decanted and the saturated PBP resin was resuspended into a Tris buffer (10 mM Tris-HCl, 1 mM $MgCl_2$) at pH 8, 10, or 12 for 10 min. All experiments were conducted at 25 °C.

2.5. Kinetic modeling

Adsorption kinetics generally follow pseudo-first order (PFO) or pseudo-second order (PSO) models (Revellame et al., 2020). The fit of both models was evaluated for the adsorption data in this study. The nonlinear forms of the PFO and PSO models are shown in Eqs. (1) and (2), respectively (the linear forms are shown in the supplementary information [SI]):

$$q_t = q_e(1 - e^{-K_{PFO}\ t}) \tag{1}$$

$$q_t = \frac{q_e^2\ K_{PSO}\ t}{q_e\ K_{PSO}\ t\ +\ 1} \tag{2}$$

where, q_e = adsorption of sNRP at equilibrium (nmol P/nmol PBP),

q_t = adsorption capacity of sNRP at time t in min (nmol P/nmol PBP),
K_{PFO} = pseudo-first order rate constant (1/min), and
K_{PSO} = pseudo-second order rate constant (nmol PBP/nmol P-min).

2.6. Isotherm modeling

Adsorption data were fit to the Langmuir and Freundlich isotherm models, the nonlinear forms of which are shown in Equations (3) and (4), respectively (the linear forms are shown in the SI).

$$q_e = \frac{q_{max}\ K_L\ C_e}{1 + K_L\ C_e} \tag{3}$$

$$q_e = K_F\ C_e^{1/n} \tag{4}$$

where, C_e = concentration of sNRP in equilibrium (μM P),

q_{max} = maximum sNRP adsorption capacity (nmol P/nmol PBP),
K_L = Langmuir constant (1/μM P),
K_F = Freundlich constant ([nmol P/nmol PBP]*[L/μmol P]$^{1/n}$), and
n = unitless empirical constant in the Freundlich isotherm model.

2.7. Analytical methods and QA/QC

The concentrations of P_i and sNRP were measured immediately after adsorption or desorption experiments in accordance with APHA (2012) standard methods for ascorbic acid P_i (4500-P E) and TP (4500-P B) analyses by means of absorbance at 880 nm (Agilent Technologies, Santa Clara, CA, USA). The minimum detection limit (MDL) for the P_i and TP tests was 0.017 and 0.015 mg P/L, respectively, as determined following the EPA method (EPA, 2016). Phosphorus-free storage buffer blanks (10 mM Tris-HCl, 1 mM $MgCl_2$, pH 7) were used for all P_i and TP analyses. All experiments were run in triplicate. Statistical analysis was performed using two-way ANOVA and Tukey post hoc tests ($\alpha = 0.05$) using GraphPad Prism 9.3.1 (GraphPad Software Inc., La Jolla, CA).

3. Results and discussion

3.1. PBP binding affinity and thermodynamic feasibility for sNRP compared to P_i

The ITC K_D values indicated that, unsurprisingly, PBP (***phosphate***-binding protein) had the greatest affinity for P_i (Table 1). However, PBP was also able to bind sNRP, albeit with lesser affinity. Among the sNRP compounds, PBP exhibited the greatest affinity for PA (K_D similar to P_i) followed by BGP, HMP, and TrP.

The change in Gibb's free energy (ΔG) for each ligand pairing calculated using ΔS from the ITC results indicated thermodynamic feasibility of sNRP binding to PBP, although P_i binding was most favorable (Table 1).

Previously reported K_D values for PBP-P_i binding (Wang et al., 1997) coincide with our findings. However, previously reported ΔG values for PBP-P_i binding indicated greater thermodynamic favorability for PBP-P_i binding (−41.3 kJ/mol) (Venkiteshwaran et al., 2020). Differences in approaches between the two studies may account for the variability. For example, Venkiteshwaran et al. (2020) calculated ΔG from experimental isotherm parameters, whereas calorimetric determination of the thermodynamics of binding was performed here using ITC measurements. Moreover, the ITC experiments performed here were conducted with suspended PBP, whereas immobilized PBP was used previously (Venkiteshwaran et al., 2020). Finally, the PBP tested in the two studies may have differed in the proportion of initially available active sites as the suspended PBP used for ITC was unfolded to remove residual P_i while a pH 12 wash was used to remove residual P_i in the immobilized PBP tests.

Table 1
Thermodynamic properties of binding between phosphate-binding proteins (PBP) and soluble reactive phosphorus (sRP) or soluble nonreactive phosphorus (sNRP). The dissociation constant (K_D), change in enthalpy (ΔH), change in entropy (ΔS), and change in Gibb's free energy (ΔG) were assessed using isothermal titration calorimetry (ITC).

Classification	Compounds	K_D (μM P)	ΔH (kJ/mol)	ΔS (kJ/mol-K)	ΔG (kJ/mol)
sRP	Orthophosphate (P_i)	0.030	−14.5	8×10^{-3}	−16.9
sNRP	Phytic acid (PA)	0.031	−2.9	1×10^{-3}	−5.9
	Sodium triphosphate (TrP)	1.80	−1.6	8×10^{-3}	−4.0
	Sodium hexametaphosphate (HMP)	0.167	−0.6	9×10^{-3}	−3.4
	Beta-glycerol phosphate (BGP)	0.106	−2.6	1×10^{-3}	−5.7

3.2. Rates of sNRP adsorption on PBP resin

Given that the ITC results showed that sNRP binding on PBP was thermodynamically feasible, experiments were performed to test sNRP adsorption using PBP resin. The rate of adsorption is an important parameter in system design as more rapid adsorption kinetics allow for smaller process volume or lower hydraulic retention times.

The PSO model provided a better fit for sNRP adsorption onto PBP resin ($R^2 \geq 0.98$) compared to the PFO model ($R^2 \leq 0.69$). The non-linear PSO model is shown in Fig. 2a (the linear PFO and PSO models and associated R^2 values are shown in Fig. S1 in the SI). Similarly, Venkiteshwaran et al. (2020) showed that P_i adsorption on PBP resin followed PSO kinetics.

The relative rate of adsorption was HMP > PA > TrP > BGP. Adsorption of sNRP onto PBP was rapid (time for 95% adsorption, $t_{95\%}$, <4 min), whereas $t_{95\%}$ was approximately an order of magnitude higher, generally exceeding 30 min, for sNRP adsorption using activated carbon, carbon nanotubes, XAD resins, or La-based adsorbents (Fig. 2b) (Campos do Lago et al., 2020; Xu et al., 2020; Wang et al., 2018a, 2018b). However, with the exception of HMP, PBP-sNRP binding was slower than PBP-P_i binding, which achieved 95% adsorption in less than 1 min (Venkiteshwaran et al., 2020).

3.3. Isotherm modeling to determine capacity of PBP resin for sNRP adsorption

The Langmuir isotherm model (nonlinear model shown in Fig. 3a; linear model, $R^2 \geq 0.96$, shown in Fig. S2a) provided a better fit to the experimental data compared to the Freundlich isotherm model ($R^2 \leq 0.80$, Fig. S2b). The Langmuir isotherm model is used for adsorbents with homogeneous, identical, and energetically equivalent active adsorption sites, for which the adsorbate does not interact with other sites, and once a molecule is bound to an active site, no further binding is possible (Saadi et al., 2015). Accordingly, the strong Langmuir model fit indicates that the active protein-binding site on each PBP molecule binds one available phosphate group (either P_i or an available phosphate group in an sNRP molecule). As shown in Fig. 3b, PBP offers higher affinity for sNRP compared to sNRP affinity using XAD resins, activated carbon, carbon nanotubes, Hr-MgO, and La-based adsorbents. Notably, among the other adsorbents compared here, PAC had high affinity for triphenyl phosphate (similar order of magnitude to PBP resin, Fig. 3b), and also provided the most rapid sNRP adsorption after PBP resin (Fig. 2b).

The q_{max} values for the sNRP compounds were generally higher compared to the maximum adsorption capacity for P_i on PBP resin (0.90 nmol P_i/nmol PBP) reported by Venkiteshwaran et al. (2020). This is likely because one terminal phosphate group in an sNRP compound attached to the phosphate-binding site, but total P removal from the

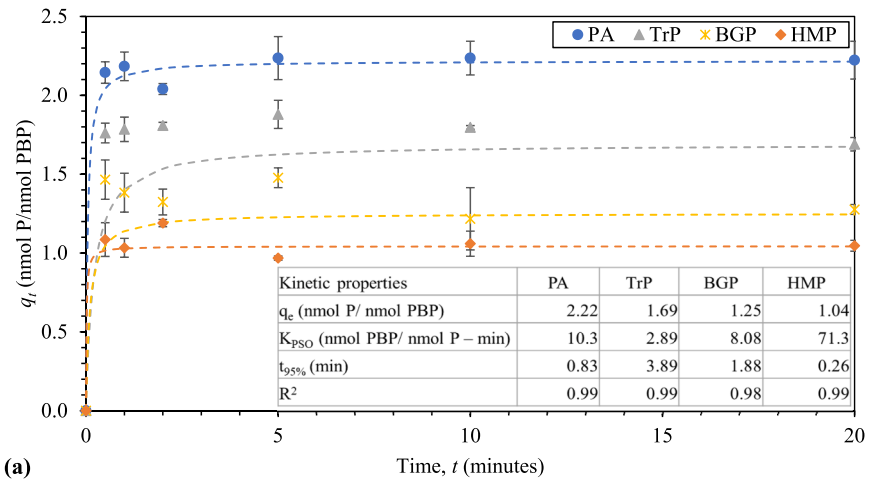

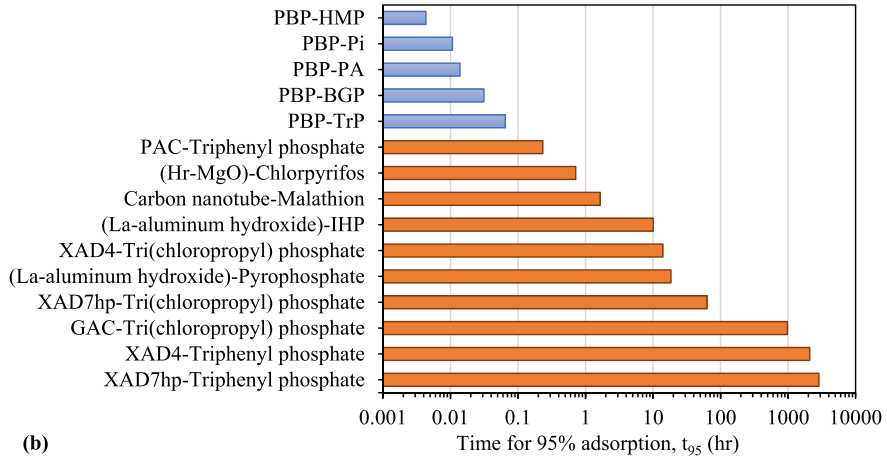

Fig. 2. (a) Pseudo-second order (PSO) kinetic model for adsorption of phytic acid (PA), sodium triphosphate (TrP), beta-glycerol phosphate (BGP), and sodium hexametaphosphate (HMP) on phosphate-binding protein (PBP) resin. Tests were run at 25 °C under neutral pH conditions. Error bars represent ±1 standard error of triplicate experiments. **(b)** Comparison of the time required to achieve 95% adsorption of P using different adsorbates (written as adsorbent-adsorbate). The blue bars show results using PBP resin to adsorb soluble non-reactive phosphorus (sNRP, this study) as well as reactive phosphorus (P_i) (Venkiteshwaran et al., 2020). The orange bars show results of other adsorbent-sNRP pairings reported in the literature (Campos do Lago et al., 2020; Xu et al., 2020; Sharma and Kakkar, 2017; Wang et al., 2018b, 2018a), all of which take longer than PBP resin to achieve the same extent of sNRP adsorption. The sNRP compound IHP was myo-inositol hexakisphosphate (Na salt of PA). (For interpretation of the references to color in this figure legend, the reader is referred to the Web version of this article.)

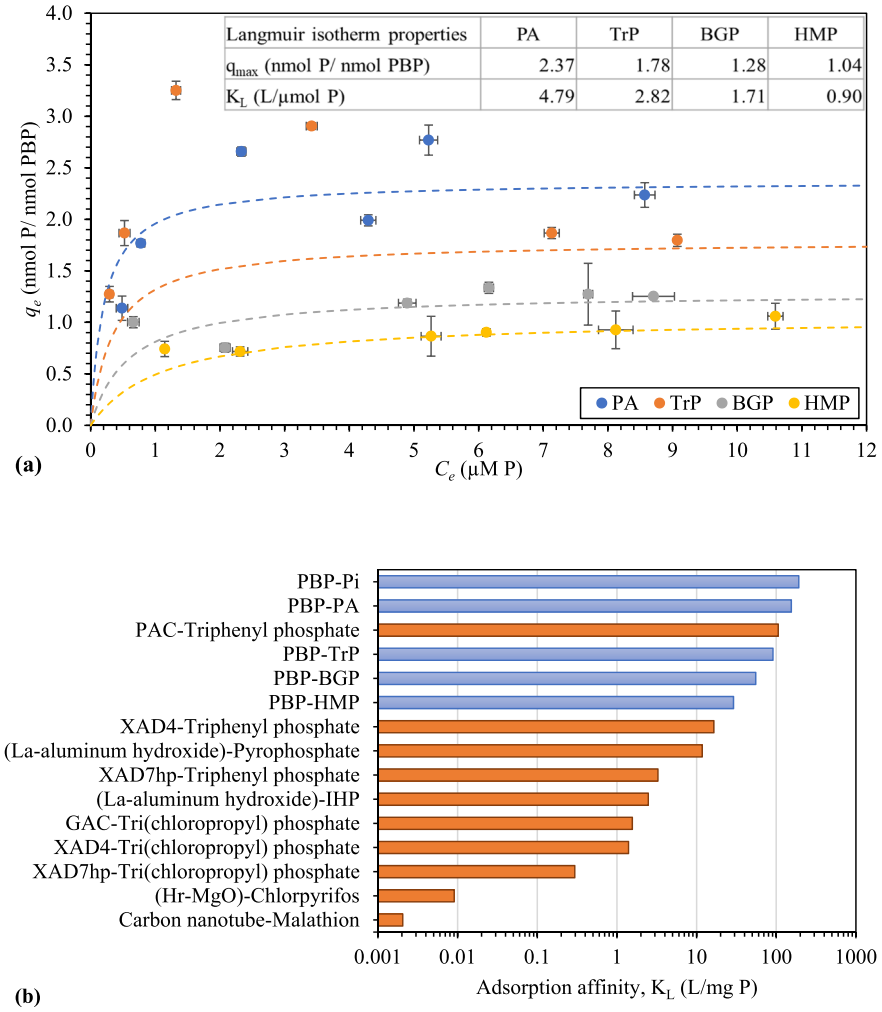

Fig. 3. (a) Langmuir isotherm model for adsorption of phytic acid (PA), sodium triphosphate (TrP), beta-glycerol phosphate (BGP), and sodium hexametaphosphate (HMP) on phosphate-binding protein (PBP) resin. Tests were run at 25 °C for 10 min under neutral pH conditions. Error bars represent ±1 standard error of triplicate experiments. **(b)** Comparison of adsorption affinity, represented as the Langmuir constant (K_L), for adsorption of different adsorbates (written as adsorbent-adsorbate). The blue bars show results using PBP resin to adsorb soluble non-reactive phosphorus (sNRP, this study) as well as reactive phosphorus (P_i) (Venkiteshwaran et al., 2020). The orange bars show results of other adsorbent-sNRP pairings reported in the literature (Campos do Lago et al., 2020; Xu et al., 2020; Sharma and Kakkar, 2017; Wang et al., 2018b, 2018a), many of which have lower sNRP binding affinity compared to PBP resin. The sNRP compound IHP was myo-inositol hexakisphosphate (Na salt of PA). (For interpretation of the references to color in this figure legend, the reader is referred to the Web version of this article.)

solution was higher given that the captured sNRP compounds contained more than one P atom. Adsorption of the sNRP compound HMP (6 P atoms) did not, however, align with this finding. Binding of HMP on the phosphate-binding site might be negatively affected by the lack of two available oxygen atoms in the terminal phosphate group, which would reduce the number of hydrogen bonds formed, and ostensibly needed for effective attachment in the protein cleft (Wang et al., 1997).

The relative order of sNRP adsorption capacity on PBP resin was PA > TrP > BGP > HMP. For comparison, suspended PBP's relative order of binding affinity was PA > BGP > HMP > TrP. This variation highlights the potential for differences in binding and removal coefficients determined using ITC (K_D, calculated from molecular binding energy) versus adsorption isotherm experiments (K_L, calculated from P removal). Although K_D and K_L can be calculated from one another, they reflect differences in determination based on objective. For example, while PBP has one to 1 M capacity for P_i binding, higher molar ratios of sNRP removal can be achieved due to higher P content in sNRP molecules. Moreover, as discussed previously, the experimental approach using ITC and adsorption experiments differed (mobilized versus immobilized PBP and unfolding versus alkaline wash to release residual P_i from the purified proteins). Accordingly, the PBP-sNRP binding energy and the actual removal capacity of sNRP using PBP resin (more representative of wastewater treatment applications) are not necessarily directly proportional.

3.4. Competition between P_i and sNRP for adsorption onto PBP resin

PBP exhibits extraordinary affinity for P_i, even relative to very similarly structured oxyanions such as arsenate (Venkiteshwaran et al., 2021b). The ITC results in this study also demonstrated that PBP has stronger affinity for P_i compared to sNRP. However, immobilized PBP's ability to adsorb sNRP even in the presence of P_i, a likely scenario in wastewater matrices, has yet to be tested. Thus, mixtures of sNRP (PA) and P_i were used to assess competitive binding on the PBP resin (Fig. 4). For solutions containing a mixture of P_i and sNRP, no significant change in P_i binding was observed regardless of the relative ratio of the compounds ($p \geq 0.2437$). This result aligns well with Poole and Hancock's (1984) finding that P_i binding using suspended PBP was not inhibited by organophosphates, even when sNRP was present at 1000-fold higher levels than P_i. However, significantly less sNRP removal resulted as the fraction of sNRP decreased from 100% to 70% and 70% to 60% ($p \leq 0.0002$). No further reduction in sNRP removal was observed when sNRP decreased from 60% to 20% ($p = 0.9711$).

As shown in Fig. 4, TP removal decreased significantly ($p = 0.0068$) when P_i was present in the bulk solution. This likely reflects preferential P_i binding, which reduces the number of sites available for sNRP; since each molecule of sNRP contains more P than a molecule of P_i, this results in less TP removal.

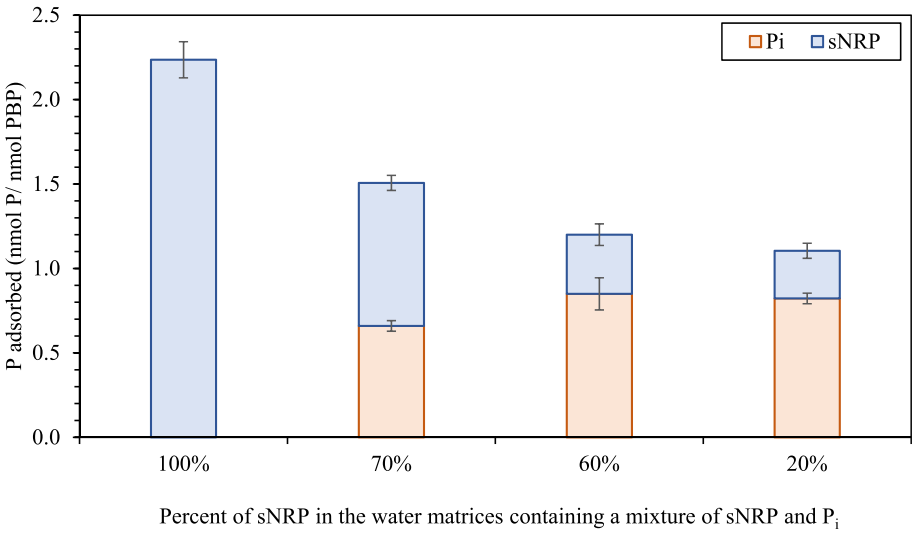

Fig. 4. Adsorption of orthophosphate (P_i) and sNRP (phytic acid [PA] was used in this test) on phosphate-binding protein (PBP) resin for solutions with varying ratios of P_i to sNRP. The total phosphorus (TP) concentration was 0.35 mg P/L in all tests. Tests were run at 25 °C for 10 min under neutral pH conditions. The error bars represent ±1 standard error of triplicate experiments.

3.5. Release of sNRP from PBP

Desorption experiments were conducted to assess the recoverability of the sNRP compounds after adsorption on the PBP resin. Venkiteshwaran et al. (2018b) previously showed that PBP released P_i as pH increased; thus, desorption of sNRP was assessed at pH 8, 10, and 12. Desorption of PA and HMP did not increase significantly from pH 8 to 10 (Fig. 5, $p \geq 0.8920$), but significantly greater desorption occurred when pH increased from 10 to 12 ($p \leq 0.0189$). Desorption of TrP and BGP did not increase significantly from pH 8 to pH 10, nor from pH 10 to pH 12 ($p \geq 0.0670$); however, desorption at pH 12 was significantly better than pH 8 ($p \leq 0.0269$). Therefore, sNRP adsorption can be performed at circumneutral pH, while desorption can be achieved at pH 12, consistent with recommendations for P_i removal and recovery (Venkiteshwaran et al., 2018b). This result further supports that the sNRP bound to the protein's phosphate-binding site (as opposed to adsorbing on the surface of PBP), which is most active at pH 5.6 to pH 7 and loses its binding activity at pH > 9 (Luecke and Quiocho, 1990; Wang et al., 1994). Via this desorption step, the sNRP can be concentrated into a smaller volume, and subsequently transformed, e.g., using electrooxidation (Mallick et al., 2021) into more readily recoverable forms for enhanced recovery of P products such as struvite.

3.6. Adsorption mechanism for sNRP binding with PBP

As shown in the previous sections, PBP-sNRP binding demonstrated similarity with PBP-P_i binding in terms of rapid binding kinetics, strong Langmuir isotherm model fit, and release of adsorbed sNRP under alkaline condition. This cumulative evidence suggests that sNRP likely bound to PBP's phosphate-binding site using the phosphate functional groups of the sNRP compounds.

When PBP binds P_i, it relies on the formation of 12 hydrogen bonds between the protein's amino acid residues and the oxygen atoms in monobasic or dibasic P_i molecules (Fig. 6). Although bacteria rely on phosphate-specific transporters (wherein PBP performs the critical initial attachment step) to uptake P_i, when P_i is not available, cells are also capable of using organophosphates (P_i esters, e.g., the organic sNRP species tested here, PA and BGP), inorganic phosphite, and phosphonates. Some organophosphates and phosphonates can enter the cell intact (Santos-Beneit et al., 2008). For example, the

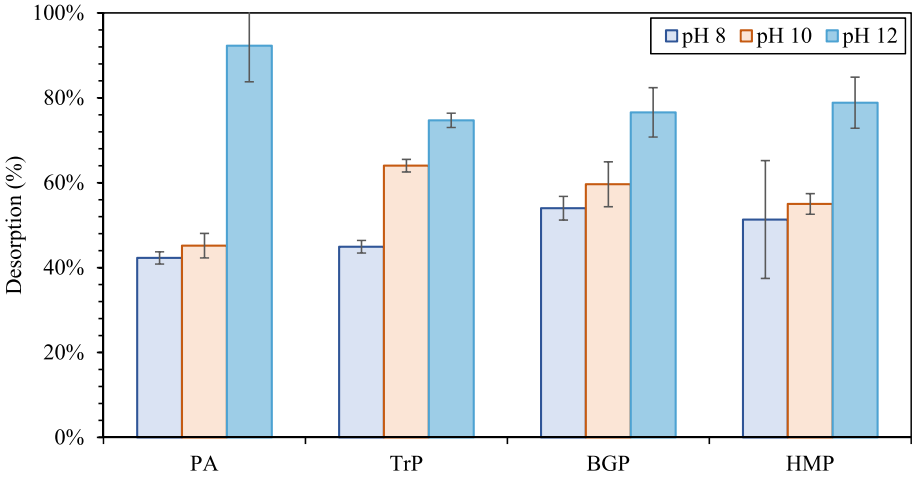

Fig. 5. Desorption of sNRP – phytic acid (PA), sodium triphosphate (TrP), beta-glycerol phosphate (BGP), and sodium hexametaphosphate (HMP) – after adsorption on phosphate-binding protein (PBP) resin. Tests were run at 25 °C for 10 min. The test compounds were first adsorbed on PBP for 10 min under neutral pH conditions, then desorbed using pH 8, 10, or 12 buffers. The bars show averages and error bars represent ±1 standard error of triplicate experiments.

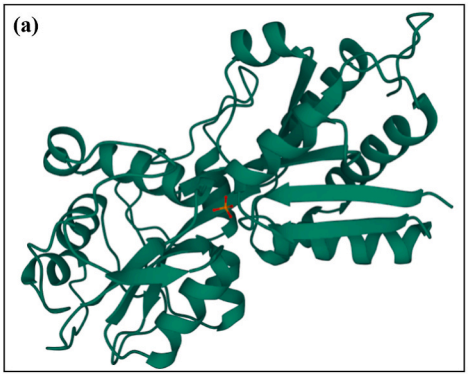

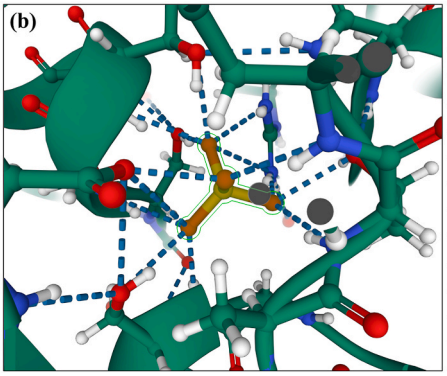

Phosphate atom	Hydrogen bond partner residue
O1	Thr 10
	Thr 10
	Arg 135
O2	Arg 135
	Ser 139
	Thr 141
	Thr 141
O3	Ser 38
	Ser 38
	Gly 140
O4	Phe 11
O4-H	Asp 56

Fig. 6. a) Phosphate-binding protein (green) complexed with phosphate (red). b) Detailed view of the ligand interaction. The phosphate molecule is bound by 12 hydrogen bonds, as specified in the table (Luecke and Quiocho, 1990). Panels a and b were created using PDB ID 1IXH as input to Mol* at www.rcb.org (Sehnal et al., 2021). (For interpretation of the references to color in this figure legend, the reader is referred to the Web version of this article.)

binding-protein-dependent Ugp transporter uptakes *sn*-glycerol-3-phosphate (G-3-P) and glycerophosphoryl diesters (whereas Pst or Pit transporters are responsible for P_i uptake) (Wanner, 1993). However, since most organophosphates are not transportable, the P_i is typically freed from the organic molecule prior to uptake, e.g., via enzymatic hydrolysis (Ohtake et al., 1998). While the phosphate-specific transport system (Pst) does not transport sNRP into cells, we hypothesize that the binding protein was able to bind accessible phosphate groups on the sNRP molecules that we tested, albeit at lower efficiency compared to P_i due to the presence of the other molecular constituents. For example, BGP's phosphate group may form hydrogen bonds between the three available oxygens and PBP residues, identically to P_i, as shown in Fig. 6, while the remaining O attached to the $C_3H_7O_2$ does not bind to the active site. Related, the availability of only a single oxygen atom in HMP may impede its PBP binding efficiency (thus yielding less P removal even though it has six phosphate functional groups). Future crystallography assessments of this binding mechanism and the structural and chemical properties of the ligand interactions are needed to further test this hypothesis.

Accordingly, sNRP structure and the availability of oxygens to bind at PBP's active site are likely to strongly influence TP removal and recovery. A combination of other ambient water quality parameters has also been shown to influence P binding using immobilized PBP, particularly pH and temperature (Venkiteshwaran et al., 2020).

4. Conclusions

Currently available P treatment technologies do not effectively remove or recover sNRP (Venkiteshwaran et al., 2018a). Previous adsorption studies targeting sNRP removal report long contact times for adsorption and low adsorption/desorption affinities (Campos do Lago et al., 2020; Xu et al., 2020; Sharma and Kakkar, 2017; Wang et al., 2018a, 2018b). The phosphate-selective PBP resin tested in this study previously demonstrated effective adsorption and desorption for P_i removal and recovery, and here we showed for the first time that the PBP resin also effectively adsorbs sNRP. While PBP has stronger affinity for P_i, adsorption of all sNRP compounds tested, including organic (phosphoester bonds), inorganic (phosphoanhydride bonds), cyclic, and noncyclic molecules, was thermodynamically feasible using PBP, with 95% of maximum adsorption occurring within 4 min.

Adsorption of the sNRP compounds followed the Langmuir isotherm model, indicating 1:1 adsorption of a phosphate group on PBP's single active site. As the PBP likely binds sNRP molecules using a single terminal phosphate, "bonus" P removal can be achieved without direct binding since some sNRP compounds contain more than one phosphate group. However, poorer removal of HMP suggests that when multiple oxygen atoms in the phosphate group are bound to other atoms, it reduces their ability to bind to the protein, and negatively affects sNRP adsorption. Compared to other adsorbents, PBP adsorbed sNRP at a higher rate with greater affinity. However, as noted by Venkiteshwaran et al. (2020) for P_i adsorption using PBP resin, the material's overall sNRP capacity was low compared to other adsorbents due to the protein's high molecular weight relative to other commonly used P-binding chemical functional groups. Future work focused on increasing the adsorption capacity of immobilized PBP materials is needed.

After adsorption on the PBP resin, controlled desorption of sNRP was achieved under high pH conditions (pH 12), demonstrating effective recoverability of the sNRP compounds. The PBP resin can thus be used to concentrate sNRP compounds for further treatment. For instance, concentrated PBP can be transformed to sRP using processes such as electrooxidation. Thus, PBP resin can contribute to a circular P economy by facilitating enhanced sNRP removal and recovery.

Credit author statement

Mallick: Conceptualization, Methodology, Validation, Formal analysis, Investigation, Writing – Original draft, Writing – Review & Editing, Visualization. **Hussein:** Methodology, Validation, Investigation, Writing – Review & Editing. **Husted:** Investigation, Writing – Review & Editing. **Mayer:** Conceptualization, Resources, Writing – Review & Editing, Visualization, Supervision, Project administration, Funding acquisition.

Declaration of competing interest

The authors declare the following financial interests/personal relationships which may be considered as potential competing interests: B. Mayer is a co-inventor on a patent application entitled "Process for controlled adsorption and desorption of phosphate from liquids using phosphate-selective proteins". The authors declare no other competing interests.

Acknowledgements

This project was supported by CAREER award 1554511 from the National Science Foundation (NSF) to B.K.M. Any opinions, findings, and conclusions or recommendations expressed in this article are those of the authors and do not necessarily reflect the views of the NSF. SH was supported by Marquette's Global Water Center: Project Water Internship Program.

Appendix A. Supplementary data

Supplementary data to this article can be found online at https://doi.

org/10.1016/j.chemosphere.2022.135311.

References

APHA, 2012. Standard Methods for the Examination of Water and Wastewater, twenty-second ed. American Public Health Association, American Water Works Association, Water Environment Federation, Washington D.C., USA.

Badawy, M.I., Ghaly, M.Y., Gad-Allah, T.A., 2006. Advanced oxidation processes for the removal of organophosphorus pesticides from wastewater. Desalination 194, 166–175. https://doi.org/10.1016/j.desal.2005.09.027.

Campos do Lago, A., da Silva Cavalcanti, M.H., Rosa, M.A., Silveira, A.T., Teixeira Tarley, C.R., Figueiredo, E.C., 2020. Magnetic restricted-access carbon nanotubes for dispersive solid phase extraction of organophosphates pesticides from bovine milk samples. Anal. Chim. Acta 1102, 11–23. https://doi.org/10.1016/J.ACA.2019.12.039.

Carpenter, S.R., 2008. Phosphorus control is critical to mitigating eutrophication. Proc. Natl. Acad. Sci. USA 105, 11039–11040. https://doi.org/10.1073/PNAS.0806112105.

Choi, S.S., Lee, H.M., Ha, J.H., Kang, D.G., Kim, C.S., Seo, J.H., Cha, H.J., 2013. Biological removal of phosphate at low concentrations using recombinant *Escherichia coli* expressing phosphate-binding protein in periplasmic space. Appl. Biochem. Biotechnol. 171, 1170–1177. https://doi.org/10.1007/s12010-013-0187-1.

Daneshvar, N., Hejazi, M.J., Rangarangy, B., Khataee, A.R., 2004. Photocatalytic degradation of an organophosphorus pesticide phosalone in aqueous suspensions of titanium dioxide. J. Environ. Sci. Health - B Pestic. Food Contam. Agric. Waste 39, 285–296. https://doi.org/10.1081/PFC-120030242.

Drolc, A., Zagorc Koncan, J., 2002. Estimation of sources of total phosphorus in a river basin and assessment of alternatives for river pollution reduction. Environ. Int. 28, 393–400. https://doi.org/10.1016/S0160-4120(02)00062-4.

EPA, 2016. Definition and Procedure for the Determination of the Method Detection Limit, Revision 2. https://www.epa.gov/cwa-methods.

Gray, H.E., Powell, T., Choi, S., Smith, D.S., Parker, W.J., 2020. Organic phosphorus removal using an integrated advanced oxidation-ultrafiltration process. Water Res. 182, 115968. https://doi.org/10.1016/J.WATRES.2020.115968.

Gu, A.Z., Liu, L., Neethling, J.B., Stensel, H.D., Murthy, S., 2011. Treatability and fate of various phosphorus fractions in different wastewater treatment processes. Water Sci. Technol. 63, 804–810. https://doi.org/10.2166/wst.2011.312.

Hussein, F.B., Mayer, B.K., 2022. Fixed-bed column study of phosphate adsorption using immobilized phosphate-binding protein. Chemosphere 295. https://doi.org/10.1016/j.chemosphere.2022.133908.

Kuroda, A., Kunimoto, H., Morohoshi, T., Ikeda, T., Kato, J., Takiguchi, N., Miya, A., Ohtake, H., 2000. Evaluation of phosphate removal from water by immobilized phosphate-binding protein PstS. J. Biosci. Bioeng. 90, 688–690. https://doi.org/10.1263/jbb.90.688.

Li, Q., Yu, Z., Shao, X., He, J., Li, L., 2009. Improved phosphate biosorption by bacterial surface display of phosphate-binding protein utilizing ice nucleation protein. FEMS (Fed. Eur. Microbiol. Soc.) Microbiol. Lett. 299, 44–52. https://doi.org/10.1111/j.1574-6968.2009.01724.x.

Luecke, H., Quiocho, F.A., 1990. High specificity of a phosphate transport protein determined by hydrogen bonds. Nature 347 (6291), 402–406. https://doi.org/10.1038/347402a0.

Mallick, S.P., Ryan, D.R., Venkiteshwaran, K., McNamara, P.J., Mayer, B.K., 2021. Electro-oxidation to convert dissolved organic nitrogen and soluble non-reactive phosphorus to more readily removable and recoverable forms. Chemosphere 279. https://doi.org/10.1016/j.chemosphere.2021.130876.

Mayer, B.K., Baker, L.A., Boyer, T.H., Drechsel, P., Gifford, M., Hanjra, M.A., Parameswaran, P., Stoltzfus, J., Westerhoff, P., Rittmann, B.E., 2016. Total value of phosphorus recovery. https://doi.org/10.1021/acs.est.6b01239.

Morse, G.K., Brett, S.W., Guy, J.A., Lester, J.N., 1998. Review: phosphorus removal and recovery technologies. Sci. Total Environ. 212, 69–81. https://doi.org/10.1016/S0048-9697(97)00332-X.

Ohtake, H., Kato, J., Kuroda, A., Wu, H., Ikeda, T., 1998. Regulation of bacterial phosphate taxis and polyphosphate accumulation in response to phosphate starvation stress. J. Biosci. 23, 491–499. https://doi.org/10.1007/BF02936143.

Poole, K., Hancock, R.E.W., 1984. Phosphate transport in Pseudomonas aeruginosa. Eur. J. Biochem. 144, 607–612. https://doi.org/10.1111/j.1432-1033.1984.tb08508.x.

Qin, C., Liu, H., Liu, L., Smith, S., Sedlak, D.L., Gu, A.Z., 2015. Bioavailability and characterization of dissolved organic nitrogen and dissolved organic phosphorus in wastewater effluents. Sci. Total Environ. 511, 47–53. https://doi.org/10.1016/j.scitotenv.2014.11.005.

Reijnders, L., 2014. Phosphorus resources, their depletion and conservation, a review. Resour. Conserv. Recycl. 93, 32–49. https://doi.org/10.1016/j.resconrec.2014.09.006.

Revellame, E.D., Fortela, D.L., Sharp, W., Hernandez, R., Zappi, M.E., 2020. Adsorption kinetic modeling using pseudo-first order and pseudo-second order rate laws: a review. Clean. Eng. Technol. 1, 100032. https://doi.org/10.1016/J.CLET.2020.100032.

Saadi, R., Saadi, Z., Fazaeli, R., Fard, N.E., 2015. Monolayer and multilayer adsorption isotherm models for sorption from aqueous media. Kor. J. Chem. Eng. 32, 787–799. https://doi.org/10.1007/s11814-015-0053-7.

Santos-Beneit, F., Rodríguez-García, A., Franco-Domínguez, E., Martín, J.F., 2008. Phosphate-dependent regulation of the low- and high-affinity transport systems in the model actinomycete *Streptomyces coelicolor*. Microbiology 154, 2356–2370. https://doi.org/10.1099/mic.0.2008/019539-0.

Sehnal, D., Bittrich, S., Deshpande, M., Svobodová, R., Berka, K., Bazgier, V., Velankar, S., Burley, S.K., Koča, J., Rose, A.S., 2021. Mol* Viewer: modern web app for 3D visualization and analysis of large biomolecular structures. Nucleic Acids Res. 49, W431–W437. https://doi.org/10.1093/nar/gkab314.

Sharma, L., Kakkar, R., 2017. Hierarchical porous magnesium oxide (Hr-MgO) microspheres for adsorption of an organophosphate pesticide: kinetics, isotherm, thermodynamics, and DFT studies. ACS Appl. Mater. Interfaces 9, 38629–38642. https://doi.org/10.1021/acsami.7b14370.

Sindelar, H.R., Lloyd, J., Brown, M.T., Boyer, T.H., 2016. Transformation of dissolved organic phosphorus to phosphate using UV/H_2O_2. Environ. Prog. Sustain. Energy 35, 680–691. https://doi.org/10.1002/ep.12272.

Venkiteshwaran, K., Kennedy, E., Graeber, C., Mallick, S.P., McNamara, P.J., Mayer, B. K., 2021a. Conversion of soluble recalcitrant phosphorus to recoverable orthophosphate form using UV/H2O2. Chemosphere 278. https://doi.org/10.1016/j.chemosphere.2021.130391.

Venkiteshwaran, K., McNamara, P.J., Mayer, B.K., 2018a. Meta-analysis of non-reactive phosphorus in water, wastewater, and sludge, and strategies to convert it for enhanced phosphorus removal and recovery. Sci. Total Environ. https://doi.org/10.1016/j.scitotenv.2018.06.369.

Venkiteshwaran, K., Pokhrel, N., Hussein, F., Antony, E., Mayer, B.K., 2018b. Phosphate removal and recovery using immobilized phosphate binding proteins. Water Res. X 1, 100003. https://doi.org/10.1016/j.wroa.2018.09.003.

Venkiteshwaran, K., Wells, E., Mayer, B.K., 2021b. Immobilized phosphate-binding protein can effectively discriminate against arsenate during phosphate adsorption and recovery. Water Environ. Res. 93, 1173–1178. https://doi.org/10.1002/WER.1498.

Venkiteshwaran, K., Wells, E., Mayer, B.K., 2020. Kinetics, affinity, thermodynamics, and selectivity of phosphate removal using immobilized phosphate-binding proteins. Environ. Sci. Technol. 54, 10885–10894. https://doi.org/10.1021/ACS.EST.0C02272.

Wanner, B.L., 1993. Gene regulation by phosphate in enteric bacteria. J. Cell. Biochem. 51, 47–54. https://doi.org/10.1002/jcb.240510110. PMID: 8432742.

Wang, W., Deng, S., Li, D., Ren, L., Shan, D., Wang, B., Huang, J., Wang, Y., Yu, G., 2018a. Sorption behavior and mechanism of organophosphate flame retardants on activated carbons. Chem. Eng. J. 332, 286–292. https://doi.org/10.1016/J.CEJ.2017.09.085.

Wang, W., Deng, S., Li, D., Ren, L., Wang, B., Huang, J., Wang, Y., Yu, G., 2018b. Adsorptive removal of organophosphate flame retardants from water by non-ionic resins. Chem. Eng. J. 354, 105–112. https://doi.org/10.1016/J.CEJ.2018.08.002.

Wang, Z., Choudhary, A., Ledvina, P.S., Quiocho, F.A., 1994. Fine tuning the specificity of the periplasmic phosphate transport receptor. Site-directed mutagenesis, ligand binding, and crystallographic studies. J. Biol. Chem. 269, 25091–25094. https://doi.org/10.1016/S0021-9258(17)31503-X.

Wang, Z., Luecke, H., Yao, N., Quiocho, F.A., 1997. A low energy short hydrogen bond in very high resolution structures of protein receptor-phosphate complexes. Nat. Struct. Biol. 1997 (4), 519–522. https://doi.org/10.1038/nsb0797-519.

Xu, R., Lyu, T., Zhang, M., Cooper, M., Pan, G., 2020. Molecular-level investigations of effective biogenic phosphorus adsorption by a lanthanum/aluminum-hydroxide composite. Sci. Total Environ. 725, 138424. https://doi.org/10.1016/j.scitotenv.2020.138424.

Yang, Y., Ballent, W., Mayer, B.K., 2016. High-affinity phosphate-binding protein (PBP) for phosphorous recovery: proof of concept using recombinant Escherichia coli. FEMS Microbiol. Lett. 363, fnw240. https://doi.org/10.1093/femsle/fnw240.